

专题——基于团簇理论的薄膜成分设计

Chemical Formulas of Cr-doped Diamond-like Amorphous Carbon Possessing High Corrosion Resistance and Electrical Conductivity

WU Ai-min^{a,b}, WANG Tong^a, WANG Qing^a, LIN Guo-qiang^{a,b}, DONG Chuang^a

(a.Key Laboratory of Materials Modification by Laser, Ion, and Electron Beams (Ministry of Education);

b.Key Laboratory of Energy Materials and Devices (Liaoning Province), School of Materials Science and Engineering, Dalian University of Technology, Dalian 116024, China)

ABSTRACT: Cr-doped diamond-like amorphous carbon, possessing good electrical conductivity and corrosion resistance, are especially important for bipolar plates coating for fuel cells. The present work addresses its amorphous structure using the cluster-plus-glue-atom model, where a good glass forming materials described by a structural unit covering a characteristic nearest-neighbor cluster plus a few next-shell glue atoms. According to the literature, the prevailing cluster in Cr-doped diamond-like amorphous carbon is Cr-centered and C-shelled $[\text{Cr-C}_4]$ tetrahedral cluster. Then, this cluster is matched with appropriate glue atoms to satisfy the electron orbital saturation principle. Two composition formulas are thus proposed, $[\text{Cr-C}_4]\text{CrC}_3(22.2\text{at.}\%\text{Cr})$ and $[\text{Cr-C}_4]\text{Cr}_3\text{C}_2(40\text{at.}\%\text{Cr})$ that show good amorphous structural stabilities. It is pointed out that the coatings of the proposed chemical compositions show simultaneously low electrical resistivity (down to $10^{-4}\Omega\cdot\text{cm}$) and superior corrosion resistance (corrosion current density $\sim 10^{-2}\mu\text{A}/\text{cm}^2$). The synergetic electrical and corrosion behavior is discussed within the framework of sp^2 bond content and of the percolation theory. This work verifies the feasibility of the cluster-plus-glue-atom model in composition design of coatings with high corrosion resistance and electrical conductivity.

KEY WORDS: bipolar plate coating; Cr doping DLC; cluster-plus-glue-atom model; electrical resistivity

中图分类号: TG174.4 文献标识码: A 文章编号: 1001-3660(2020)05-0001-10

DOI: 10.16490/j.cnki.issn.1001-3660.2020.05.001

具有高耐蚀性和导电性的掺 Cr 类 金刚石非晶碳的化学式解析

吴爱民^{a,b}, 王同^a, 王清^a, 林国强^{a,b}, 董闯^a

(大连理工大学 材料科学与工程学院 a.三束材料改性教育部重点实验室,
b.辽宁省能源材料及器件重点实验室, 辽宁 大连 116024)

收稿日期: 2020-01-03; 修订日期: 2020-04-10

Received: 2020-01-03; Revised: 2020-04-10

基金项目: 国家重点研发计划项目 (2016YFB0101206)

Fund: Supported by the National Key Research and Development Program of China (2016YFB0101206)

作者简介: 吴爱民 (1973—), 男, 博士, 副教授, 主要研究方向为能源材料及器件。

Biography: WU Ai-min (1973—), Male, Doctor, Associate professor, Research focus: energy materials and devices.

通讯作者: 董闯 (1963—), 男, 博士, 教授, 主要研究方向为合金相成分设计与材料改性。邮箱: dong@dlut.edu.cn

Corresponding author: DONG Chuang (1963—), Male, Doctor, Professor, Research focus: alloy phase composition design and material modification.

E-mail: dong@dlut.edu.cn

引文格式: 吴爱民, 王同, 王清, 等. 具有高耐蚀性和导电性的掺 Cr 类金刚石非晶碳的化学式解析[J]. 表面技术, 2020, 49(5): 1-10.

WU Ai-min, WANG Tong, WANG Qing, et al. Chemical formulas of Cr-doped diamond-like amorphous carbon possessing high corrosion resistance and electrical conductivity[J]. Surface technology, 2020, 49(5): 1-10.

摘 要: Cr 掺杂的类金刚石非晶碳具有良好的导电性和耐腐蚀性, 这对于燃料电池金属双极板涂层改性特别重要。使用团簇加连接原子模型对其非晶结构进行了详细解析, 在该模型中, 良好的玻璃形成材料由覆盖特征性最近邻团簇加上几个下一壳层原子的结构单元来表述。根据文献, 在 Cr 掺杂的类金刚石非晶碳中占优势的团簇是 Cr 中心和 C 壳层的[Cr-C₄]四面体团簇, 然后将该团簇与适当的连接原子匹配, 以满足电子轨道饱和原理。由此推导出了两个最优组成式, 即[Cr-C₄]CrC₃ (22.2%Cr) 和[Cr-C₄]Cr₃C₂ (40%Cr), 它们显示出良好的非晶态结构稳定性。实验结果显示, 所提出的这两组化学组成的涂层材料兼具低电阻率 (低至 $10^{-4} \Omega \cdot \text{cm}$) 和优异的耐腐蚀性 (腐蚀电流密度 $\sim 10^{-2} \mu\text{A}/\text{cm}^2$)。在 sp^2 键含量和渗流理论的框架内讨论了导电和耐蚀的协同行为。这项工作验证了团簇加连接原子模型在具有高耐腐蚀性和高导电性的涂层材料成分设计中的可行性。

关键词: 金属双极板涂层; Cr 掺杂 DLC 膜; 团簇加连接原子模型; 电阻率

1 Introduction

Bipolar plates made of stainless steels are a key structural part in proton exchange membrane fuel cells, constituting 60%~70% of the total mass and approximately 30% of the total stack cost^[1]. To separate the oxidants from fuels and to collect current, they require both corrosion resistance and electrical conductivity. However, the formation of a thick Cr_2O_3 layer on the stainless steel surface during the corrosion process (generally called passivation) significantly decreases the electrical conductivity. For every $25 \text{ m}\Omega \cdot \text{cm}^2$ increase in interface contact resistance, the battery power would lose 2%~5%^[2]. It has been proved^[3-5] that the service lifetime of stainless steel bipolar plates (interfacial contact resistance of $768.2 \text{ m}\Omega \cdot \text{cm}^2$ under 1.2 MPa pressure and corrosion current density of $16.2 \mu\text{A}/\text{cm}^2$ in 0.5 mol/L $\text{H}_2\text{SO}_4 + 0.0005\% \text{F}^-$ solution) can be improved by coating with metal-doped diamond-like carbons (Me-DLCs). A Cr-DLC coating, containing a quite high doping level up to ~23at.%Cr, shows superior interfacial contact resistance ($2.8 \text{ m}\Omega \cdot \text{cm}^2$ under 1.2 MPa pressure) and corrosion current density ($9.1 \times 10^{-2} \mu\text{A}/\text{cm}^2$ in 0.5 mol/L $\text{H}_2\text{SO}_4 + 0.0005\% \text{F}^-$ solution)^[3]. A W-DLC coating, with 17.3at.%W, shows slightly inferior properties (interfacial contact resistance of $6.53 \text{ m}\Omega \cdot \text{cm}^2$ under 1.5 MPa pressure and corrosion current density of $0.6 \mu\text{A}/\text{cm}^2$ in 0.5 mol/L $\text{H}_2\text{SO}_4 + 0.0002\% \text{F}^-$ solution)^[4]. An Ag-DLC coating, with 0.31at.%Ag, also show similar properties (interfacial contact resistance of $21.6 \text{ m}\Omega \cdot \text{cm}^2$ at 1.2 MPa pressure), which is more than 15 times that of the stainless steel substrate) and corrosion current density of $6 \mu\text{A}/\text{cm}^2$ in 0.5 mol/L $\text{H}_2\text{SO}_4 + 0.0005\% \text{F}^-$ solution)^[5]. Table 1 lists the doping results of some Me-DLC coatings, including the doping elements and their contents, synthesis techniques, intensity ratios of the D peak to the G peak (I_D/I_G), and electrical resistivity data^[6-12]. I_D/I_G is a parameter characterizing the DLC structure: the increase of I_D/I_G

indicates the increase of sp^2 hybrid bond content^[13]. The electrical resistivity is sensitive to the content of sp^2 hybrid bonds. The π states in sp^2 hybrid bonds form tailing states that link valence band and conduction band in the mobility gap. This leads to delocalized π -state electrons and henceforth to increased conductive electrons.

Among the many doping elements, Cr deserves a special attention due to its low electrical resistivity ($1.29 \times 10^{-5} \Omega \cdot \text{cm}$) and intrinsic passivation against corrosion. Its high chemical affinity with carbon facilitates the formation of chromium-carbide-like local structures of high stability at the atomic scale^[14]. Proper doping of Cr in DLC (Cr-DLC) increases sp^2 hybrid bonds and reduces internal stress^[6-7]. It is already proved^[3] that coating adherence, electrical conductivity, and corrosion resistance can be synergetically enhanced in Cr-DLCs. Cr-DLC has been considered as the major coating material on stainless steel bipolar plates for use in proton exchange fuel cells. Table 1 is further explored by relating the I_D/I_G ratios (sp^2 hybrid bond contents) and electrical resistivity ρ to the doping contents (Fig.1). We remark the following doping-induced phenomena: 1) with increasing doping contents, sp^2 bond generally increases while electrical resistivity ρ decreases; 2) Cr-DLCs shows the most pronounced drop of ρ upon sufficient Cr doping, by several orders of magnitude, down to a quite low level ($\sim 10^{-4} \Omega \cdot \text{cm}$), and 3) experiments on Cr-DLC coatings with doping contents above 20at.%Cr are scarce. It is therefore interesting to determine the proper doping contents of Cr, especially above 20at.%Cr, to reach a good combination of electrical resistivity and corrosion resistance. Such coatings should satisfy two basic requirements, i.e., being sufficiently stable (for anti-corrosion and strength concerns) and at the same time containing a high level of sp^2 hybrid bonds (for assuring good electrical conductivity). In fact, Wu *et al.*^[3] experimentally investigated the interface contact resistivity between carbon paper and 316L stainless steel substrate coated with Cr-DLC. They

Table 1 Characteristic parameters of metal-doped DLC coatings, including doping elements, synthesis techniques, doping contents (at.%), I_D/I_G ratios, and electrical resistivity values $\rho(\Omega\cdot\text{cm})$. In the case of square resistance R_{\square} data (Ω), the resistivity ρ is obtained via $\rho=R_{\square}\cdot d$, d (cm) being the film thickness

Doping elements, synthesis techniques	Doping contents/at. %	I_D/I_G	Electrical resistivity $\rho/(\Omega\cdot\text{cm})$
Cr-DLC, RF diode sputtering ^[6]	3.6	0.80	7.25×10^2
	4.2	1.14	1.46×10^1
	5.3	1.08	6.68×10^1
	6.6	1.34	1.38×10^{-1}
	6.5	1.56	1.59×10^{-2}
	19.5	3.20	7.31×10^{-4}
Cr-DLC, arc deposition ^[7]	25.1	0.76	4.84×10^{-4}
	4.0	1.5	3.50×10^4
	6.9	2.9	1.96×10^1
Zn-DLC, laser deposition ^[8]	10.0	3.6	2.31×10^{-1}
	0	0.30	5.00
	3	0.44	1.80×10^{-2}
	5	0.49	1.70×10^{-2}
Ti-DLC, filtered arc deposition ^[9]	10	0.74	1.35×10^{-3}
	0	1.39	3.15×10^{-1}
	1.1	1.47	7.60×10^{-2}
	4.1	1.53	1.89×10^{-1}
Ti-DLC, hybrid PVD and P-CVD ^[10]	8	1.01	1.06×10^{-1}
	15	1.15	1.25×10^{-1}
	17	1.23	1.47×10^{-1}
	18	1.33	7.69×10^{-2}
	20	2.37	5.88×10^{-2}
	30	2.78	5.56×10^{-2}
Cu-DLC, high power pulsed magnetron sputtering ^[11]	46	3.56	5.26×10^{-2}
	2	0.54	2.73
	15	1.04	5.83×10^{-2}
	21	1.09	9.00×10^{-4}
Gd-DLC (H-free), magnetron sputtering ^[12]	26	1.14	1.27×10^{-4}
	30	1.30	5.44×10^{-5}
	0	1.96	1.56×10^{-1}
	2.6	4.44	1.03×10^{-2}
Gd-DLC (H-containing), magnetron sputtering ^[12]	7.6	10.86	5.30×10^{-3}
	11.0	11.92	5.00×10^{-3}
	15.6	4.65	1.42×10^{-2}
	0	1.81	1.45
Gd-DLC (H-containing), magnetron sputtering ^[12]	4.2	3.49	9.71×10^{-1}
	6.8	3.70	2.90×10^{-1}
	13.5	8.30	2.66×10^{-2}
	15.0	7.88	3.30×10^{-2}
	15.4	6.49	5.37×10^{-2}

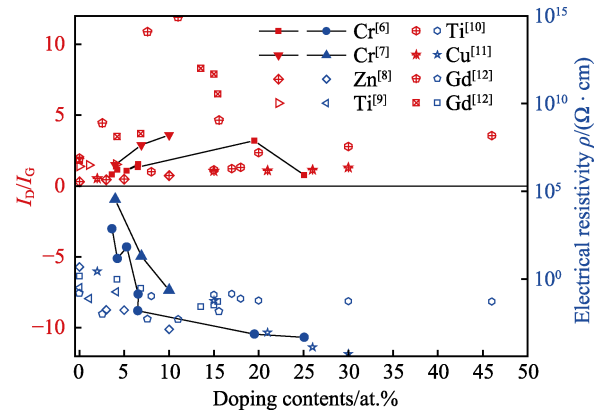


Fig.1 I_D/I_G and electrical conductivity vs. doping contents in DLC coatings^[6-12] (The data are taken from Table 1, the Cr-doped points are linked by thick lines)

found that at about 23at.%Cr, the sp^2 hybrid bond content in amorphous carbon network reaches the maximum level of 60.0%, and correspondingly, the interface contact resistance of the Cr-DLC coating is minimized.

The specific Cr-doping in DLC should be related to the structural feature of amorphous carbon. Robertson and O'Reilly^[15] proposed a two-phase model for DLC: the sp^2 hybrid bonds are embedded in carbon network consisting of sp^3 hybrid bonds. Angus *et al.*^[16] developed a completely constrained random covalent network model, believing that a dense and stable carbon network is formed when the number of constraints is equal to the atomic mechanical freedom. The former depends on the average coordination number while the latter is comparable to the dimensionality of the studied system. The bonding mode of doping elements and carbon atoms is also investigated using first-principles simulation^[17]. The 3d orbitals of Ti, W and Cr and the 3p orbitals of Al overlap with the 2p orbitals of C, forming covalent and ionic bonds. It is specially noted that, at sufficiently high doping contents, above 1.5at.%Cr, Cr and C atoms are bonded to each other in the form of a Cr-centered and four-carbon coordinated local structure^[18], expressed as $[\text{Cr-C}_4]$ cluster in the present paper. The above models are only descriptive and cannot quantitatively tell the specific composition at which DLC is stabilized.

In the present work, a short-range-order structural model, i.e., the cluster-plus-glue-atom model, is introduced in modeling the Cr-doped amorphous carbon structure. This model is actually developed from composition interpretation of bulk amorphous alloys with high glass forming abilities^[19-20]. In this model, any structure is described by a molecule-like structural unit, consisting of a nearest-neighbor coordination cluster plus a few next-shell glue atoms. This structure unit can always be expressed in the form of cluster formula, $[\text{cluster}]$ (glue atoms).

After a brief introduction on the cluster-plus-glue-atom model, the composition formulas of Cr-DLCs are first proposed. The formulas are then verified by analyzing the experimental results on electrical resistivity and corrosion resistance, both of our own and from the literature. The synergetic effect of Cr doping on electrical resistivity and corrosion resistance is finally discussed in terms of bond contents and percolation theory.

2 The cluster-plus-glue-atom model and composition interpretation of Cr-DLCs

2.1 The cluster-plus-glue-atom model

Traditional crystallography uses unit cell as the basic unit to describe atomic arrangement in solid materials. The atomic positions within the cell are provided. However, for non-crystalline structures, the crystallography mean fails largely as the periodic framework is missing. Even for crystals of large unit cells, their atomic structure description becomes a long list of atomic coordinates, lacking simplicity and physical stability. Historically several atomic structural models^[21-25] have been developed for glasses such as random network, dense random packing of hard spheres, stereo-chemical model, efficient cluster packing model and quasi-equivalent cluster model, but they are all insufficient in dealing with the quantitative composition interpretation of glassy states of high structural stabilities because the electron structure stabilization is basically missing.

Dong *et al.*^[19] proposed the cluster-plus-glue-atom model that simplifies any short-range-order atomic structure into a local structural unit covering only a nearest-neighbor cluster plus a few next-shell glue atoms distributed between the clusters. Such a local unit is then expressed by a universal cluster formula, [cluster] (glue atoms). For a metallic glass with high glass forming ability, the number of glue atoms is either 1 or 3. It has been verified that the cluster formula of a good metallic glass former always satisfies 24-electron rule^[26], i. e., the number of valence electrons per unit formula, e/u is universally 24. This special valence electron number, mimicking the octet rule in molecular substances, unveils the simple fact that an amorphous state is stabilized via electron orbital saturation principle. For example, the bulk glass composition $\text{Cu}_{64}\text{Zr}_{36}$ conforms to a cluster formula $[\text{Cu-Cu}_7\text{Zr}_5]\text{Cu}$, where the square-bracketed part represents the Cu-centered nearest-neighbor cluster derived from devitrification Cu_8Zr_3 , glued with one Cu atom to meet the 24-electron rule^[27].

2.2 Structure model and cluster formula of Cr-DLCs

As already mentioned, Cr-DLC amorphous structure

is characterized by a carbide-like local structure embedded in the amorphous carbon network. According to Andersson *et al.*^[28], who prepared Cr-DLC coatings with 15at.%, 33at.%, 50at.%, 57at.% and 75at.% Cr by DC magnetron sputtering and fully characterized them using X-ray diffraction (XRD), X-ray photoelectron spectroscopy (XPS), transmission electron microscopy (TEM), extended X-ray absorption fine structure (EXAFS), Cr—C and C—C bonds are identified and the amorphous structure can be simplified into amorphous CrC_x nanocrystals in amorphous carbon. What is important is that the coordination number of Cr—C falls close to 4^[29], or expressed in terms of cluster $[\text{Cr-C}_4]$. Singh *et al.*^[18] pointed out that Cr-rich carbide-like local structure is formed when the doping level is above 1.5at.%Cr, and the coordination number centered by Cr is nearly 4 (for 11.80at.%Cr sample, the coordination number of Cr is 3.9. The former depends on the average coordinatively). It can be easily deduced from their experimental results that, by assuming the Goldschmidt atomic radius for Cr, 0.128 nm, the atomic radius of C is $0.218-0.128=0.090$ nm, which is very close to the Goldschmidt radius of C, 0.092 nm. Therefore, in the subsequent calculations, we adopt the Goldschmidt radii of the two elements directly. Fan *et al.*^[30] studied Cr-DLC coatings by using z-contrast imaging and electron energy loss spectroscopy. They observed uniform distribution of Cr in DLC matrix at lower doping levels (~6at.%Cr) and Cr-rich clusters at higher levels (~12at.%Cr). According to Santana *et al.*^[31], Cr shows chemical states similar to Cr_3C_2 compound. Cr_3C_2 -like nanoclusters are formed in the amorphous carbon matrix when the amount of Cr doping exceeds 11.31at.%Cr^[32-33]. The existence of Cr—C bonds is also confirmed by others^[34-36]. At high Cr doping contents of 29.14at.%~49.36at.%Cr, the coatings can still maintain amorphous^[37], but crystals such as CrC (NaCl structure) can sometimes be identified^[38].

In summary, upon sufficient Cr doping, Cr-DLC structure is characterized by a carbide-like local structure, with average coordination number centered by Cr is closely 4. Therefore, we adopt the cluster $[\text{Cr-C}_4]$ for the construction of the cluster formulas for stable Cr-DLC structures. The Cr—C nearest neighborhood is also favored by the intense negative enthalpy of mixing between Cr and C (−61 kJ/mol). Actually, a similar tetrahedral configuration $[\text{Cr-C}_4]$ is also present in the atomic structure of Cr_7C_3 . According to the cluster-plus-glue-atom model, the general cluster formula for the amorphous structure of Cr-DLC coatings are then expressed as $[\text{Cr-C}_4]\text{Cr}_x\text{C}_y$. In the following, we will define precisely the glue atoms under the electron orbital saturation principle.

In the Cr-DLC structure, the electron orbitals of Cr atoms tend to overlap with the ones of C atoms in order

to form Cr—C bonding. In order to achieve the stable electron orbital configuration, mimicking the octet electron rule for chemical molecules, both electron orbitals should be saturated, respectively to reach the fully occupied states of $3d^{10}4s^2$ and $2s^22p^6$. In a stable structural unit formulated by $[\text{Cr-C}_4]\text{Cr}_xC_y$, the cluster part $[\text{Cr-C}_4]$ itself never satisfies the electron saturation rule. The total number of valence electrons of the cluster is $6+4\times4=22$, which cannot saturate both the central Cr (requiring 12 electrons to reach $3d^{10}4s^2$) and the shell atoms C_4 (requiring multiples of 8 to reach $2s^22p^6$ but only 10 electrons are left and would require 6 more electrons to reach a stable state). If the number of glue atoms is set to be equal or smaller than that of the cluster part (this is a reasonable assumption because the cluster should be the major part of the structure in the cluster-plus-glue-atom model), there are two possibilities for the glue atoms to satisfy the electron saturation rule, either Cr_1C_3 or Cr_3C_2 . In the former case, the glue atoms provide $6+3\times4=18$ electrons, which saturate both the $3d4s$ orbitals of the Cr glue atom (exhausting 12 from 18 from the glue atoms) and the $2s2p$ orbitals of all carbon atoms (10 electrons from the cluster part plus remaining 6 from the glue atoms). The total number of valence electrons is therefore $e/u=40$, which is interestingly a multiple of 8. In the latter case, the glue atoms provide $3\times6+2\times4=26$ electrons. Together with the 10 electrons from the cluster part, the 36 electrons can be regarded as being completely exhausted by the three Cr glue atoms and all the carbon atoms are just electron donors. Its $e/u=48$, again a multiple of 8. The resultant structural unit, formulated as $[\text{Cr-C}_4]\text{CrC}_3=\text{Cr}_{22.2}\text{C}_{77.8}$ and $[\text{Cr-C}_4]\text{Cr}_3\text{C}_2=\text{Cr}_{40}\text{C}_{60}$, are reminiscent of the molecular formula for chemical substances. In fact, in a recent work, we have identified the cluster formulas of typical inorganic compounds and the formulas all satisfy the electron saturation rule, as exemplified by $[\text{Si-O}_4]\text{Si}$ ($e/u=32$) for different SiO_2 quartz structures^[39]. It is expected that the corresponding amorphous structure possess good structural stabilities and henceforth high corrosion resistance and mechanical strength.

3 Experimental verification of the proposed formulas

3.1 Experiments

Amorphous Cr-DLC coatings contain a large number of sp^3 hybrid bonds that ensure their excellent chemical stability. Besides, Cr itself has good corrosion resistance, making Cr-DLC coatings good candidates for anti-corrosion purposes, such as in fuel cell bipolar plates, biological devices, lithography circuit boards, etc. However, due to experimental difficulties in the

doping content control, so far there is no sufficient experimental evidence for specific Cr doping contents, especially at high doping levels, that lead to Cr-DLCs of simultaneous low corrosion resistance and high electrical conductivity. For this objective, we carry out an experiment on preparing Cr-DLC thin films over a wide doping range and measure their corrosion and electrical conduction behavior.

Cr-DLC thin films are prepared on 316L stainless steel by pulsed-bias arc deposition using Cr (4 N) and graphite (4 N) arc sources. The deposition parameters are bias magnitude 347 V, frequency 20 kHz, duty ratio 65%, temperature 350 °C, time 35 min, arc currents 40~65 A for Cr and 85~110 A for graphite, different chromium-containing carbon films were formed by adjusting the graphite and chromium target currents. The chemical compositions (measured by XPS), bonding contents (by XPS and Raman Spectroscopy), electrical resistance (in contact with carbon sheet at 0.6 MPa pressure), and corrosion (by standard three-electrode electrochemical cell in 0.5 mol/L $\text{H}_2\text{SO}_4+0.0005\%\text{F}^-$ solution) results are provided in Table 2 and Fig.2.

Table 2 Characterization of the prepared Cr-DLC coatings for compositions and bonding contents

Cr content/at.%	sp^2 content/%	sp^3 content/%	sp^2/sp^3	I_D/I_G
17	46	24	1.917	1.65
21	44	24	1.833	3.43
24	45	22	2.045	3.00
30	43	21	2.048	2.29
39	31	21	1.476	1.35
52	15	10	1.500	1.69

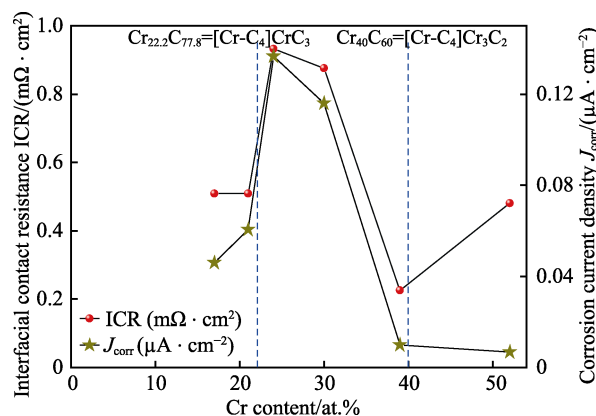


Fig.2 Interfacial contact resistance ICR and corrosion current density J_{corr} vs. Cr doping contents

The resistivity and corrosion evolution as a function of Cr contents is illustrated in Fig.2. Clearly, at the doping contents of 21at.% and 39at.%Cr, which fall close to the proposed compositions $[\text{Cr-C}_4]\text{CrC}_3 \approx \text{Cr}_{22.2}\text{C}_{77.8}$ and $[\text{Cr-C}_4]\text{Cr}_3\text{C}_2 \approx \text{Cr}_{40}\text{C}_{60}$, both interfacial contact

resistance and corrosion current density drastically fall to low levels. The results well verify the theoretical models of the stable structural units for Cr-DLC coatings. Actually the results satisfy fully the property objectives of bipolar plates for use in proton exchange fuel cell set by US Department of Energy in 2020 (corrosion current density $<1 \mu\text{A}/\text{cm}^2$ and interfacial contact resistance $<10 \text{ m}\Omega\cdot\text{cm}^2$ at 1.4 MPa pressure^[40]).

As can be seen from Table 2, the sp^2 and sp^3 bond contents as measured by XPS both decrease as Cr content increases, due to the formation of Cr-related bonds. Their relative proportions are always larger than 1, about 2 in the Cr range below 30at.%Cr and about 1.5 in the higher Cr range. This is also supported by I_D/I_G ratios that are proportional to the sp^2 contents. In particular, it is noted that, near the formulated composition 22.2at.%Cr, the sp^2 proportion reaches the highest level, $\sim 45\%$, signifying that the Cr-DLC in this region should possess a good electrical conductivity. On the other hand, near the other composition 40at.%Cr, the sp^2 proportion falls to a low level, $\sim 31\%$, while maintaining an average sp^3 level, $\sim 21\%$. The Cr-DLCs in this region are presumably less conductive but still maintain a high strength.

The bond content I_D/I_G is also related to electrical resistivity and corrosion rate, as shown in Fig.3. A small I_D/I_G ratio (i.e., low sp^2 and high sp^3 proportions in DLC) means a worsened electrical conductivity (i.e., increased ICR) and an enhanced corrosion resistance (i.e., as reflected by weak J_{corr}). However, both interfacial contact resistance and corrosion current density depend on I_D/I_G in a similar manner: both rise as I_D/I_G increases and fall again at the large I_D/I_G end. At present we do not understand why such irregularly synchronized behavior occurs. What can be remarked, nevertheless, is that the proposed formulas $[\text{Cr-C}_4]\text{CrC}_3$ (22.2at.%Cr) and $[\text{Cr-C}_4]\text{Cr}_3\text{C}_2$ (40at.%Cr) happen to possess both

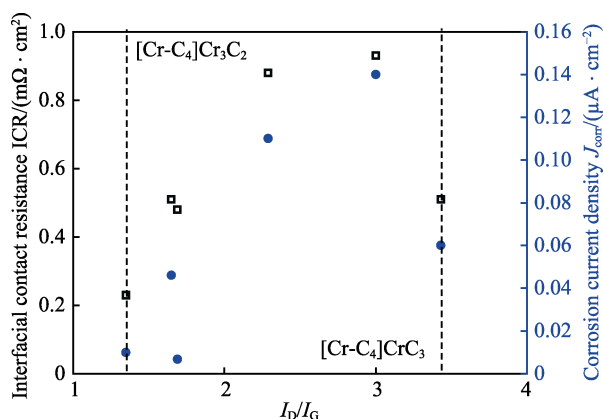


Fig.3 Interfacial contact resistance ICR ($\text{m}\Omega\cdot\text{cm}^2$, left vertical axis, open squares) and corrosion current density J_{corr} ($\mu\text{A}/\text{cm}^2$, right one, solid symbols) as a function of I_D/I_G (Two vertical dotted lines mark the special compositions of the proposed formulas)

the lowest ICR and J_{corr} , as the relevant data as marked by the dotted vertical lines are located at the two ends of the I_D/I_G range.

3.2 Analysis on corrosion data in the literature

To further support our experimental results and the proposed formulas, relevant corrosion and electrical resistivity data in the literature^[3,41-42] are collected and summarized in Fig.4, together with the data of the present work.

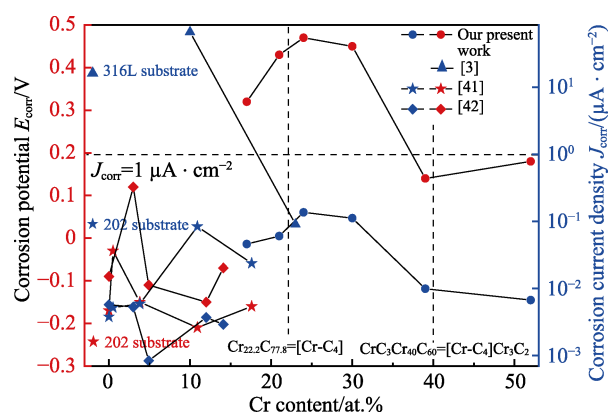


Fig.4 Relationship between corrosion resistance parameters and Cr doping contents (The data from^[3,41-42], together with those from the present work are shown. The corrosion potential (left vertical axis) and corrosion current density (right one) data are respectively indicated by blue filled symbols and by red half-filled ones. Those of the stainless steel substrates are represented by large symbols. The dotted horizontal line represents the corrosion density standard ($1 \mu\text{A}/\text{cm}^2$) set by US DOE.)

Corrosion potential and corrosion current density are generally used to quantitatively describe the chemical stability of solid materials. From a thermodynamic point of view, the corrosion potential reflects the corrosion resistance of the material, the smaller the value, the more susceptible to corrosion of the material. From a kinetic point of view, the corrosion current density reflects the corrosion rate of the material in the etching solution, the smaller the value, the slower the corrosion rate of the corresponding material.

As shown in Fig.4, the initial stainless steel substrates, no matter 316L^[3] or 202^[42], all show inferior resistances: high corrosion current densities, above $1 \mu\text{A}/\text{cm}^2$ in the case of 316L, and a negative corrosion potential nearly -0.3 V in the case of 202. The Cr-DLC coatings all exhibit improved corrosion resistance, especially in the high Cr range (above 20at.%Cr, where the corrosion potentials are all positive, in sharp contrast to those negatives ones in the lower Cr range). In particular, the films near 22.2at.%Cr have nearly the highest corrosion potential $0.4\sim 0.5 \text{ V}$ (close to that of the 316L substrate) and a corrosion current density

$\sim 10^{-1} \mu\text{A}/\text{cm}^2$ (well below the set objective of US DOE and about two orders of magnitude lower than the initial 316L substrate). This means that this coating has the least corrosion tendency, while maintaining a reasonably slow dynamic corrosion process. The near $\text{C}_{60}\text{Cr}_{40}$ coatings, on the other hand, show a lower positive corrosion potential of $\sim 0.1 \text{ V}$ but a fairly slow corrosion dynamics (corrosion current density is among the lowest, $\sim 10^{-2} \mu\text{A}/\text{cm}^2$). For the Cr-DLCs in the lower Cr range ($< 20\text{at.}\%\text{Cr}$), the corrosion current densities can be quite low but at the expense of negative corrosion potentials, implying that these coatings are easily susceptible to corrosion. It is anticipated that the coatings of the proposed compositions show sufficient corrosion resistance, suitable especially for dipolar plates.

3.3 Analysis on electrical resistivity in terms of percolation theory

In the above analysis on electrical conductivity, it is noted that the proposed Cr-DLCs, presumably stabilized due to electron saturated orbitals in the cluster-plus-glue-atom units, possess however excellent electrical conductivity, which disobeys our general belief that a stable structure should be less conductive. Since the electrical conduction is related to the presence of sp^2 bonds, here we introduce the percolation theory to explain the conduction mechanism of the Cr-DLC coatings.

Percolation theory is suitable for dealing with the effects caused by the changes in the degree of inter connection in a random system, which is widely used to describe the localized-extended states transition in amorphous networks. It is worth mentioning that the characteristic length of the system under study can span 35 orders of magnitude ($10^{-13} \sim 10^{22} \text{ cm}$)^[43]. The regular periodic lattice is composed of bonds and sites and the percolation theory correspondingly is divided into the bond percolation and the site percolation^[44].

Following the statistical characteristics of the system and randomly assigning the properties of each bond or site, a regular geometric object can be transformed into a stochastic-geometry situation. Fig.5 is a schematic diagram showing the bond and site percolations in a two-dimensional square lattice. The solid circles and the hollow circles represent “unblocked” and “blocked” sites respectively; the black lines are referred to as “connected” bonds and the parts bounded by red wireframes are called the percolation pathways.

From the perspective of bond percolation, all the sites are in the “unblocked” state, and each bond has two possible states of “connected” and “unconnected”, corresponding to probabilities p and $1-p$. When increasing the concentration of the “connected” bonds to the percolation threshold p_c in the system, a boundless

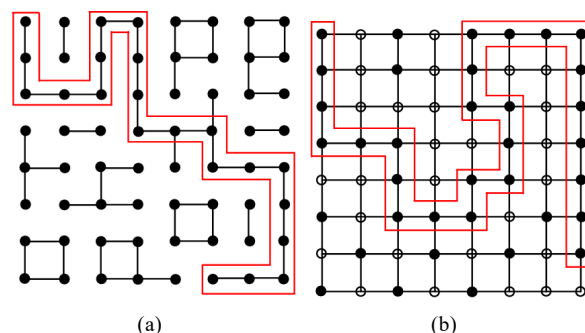


Fig.5 Bond percolation (a) and site percolation (b) in a two-dimensional square lattice (The solid circles and the hollow circles represent “unblocked” and “blocked” sites respectively, and the black lines are referred to as “connected” bonds and the parts outlined by red wireframes are called the percolation pathways.)

percolation pathway is formed. Similarly, for the site percolation, each bond is in a “connected” state with sites “unblocked” or “blocked” corresponding to probabilities p and $1-p$. In the two-dimensional square lattice configuration, the bond and site percolation thresholds are 0.500 and 0.593, respectively. In a real three dimensional atomic structure, coordination number N is the proper measure of connectivity for covalent solids, while the atomic packing factor ν (also known as packing efficiency or packing fraction, which is the fraction of spherical volume occupied by the constituent atom) is the measure of choice for metals.

As above-mentioned, we have given the cluster-plus-glue-atom formulas $[\text{Cr-C}_4]\text{CrC}_3=\text{Cr}_{22.2}\text{C}_{77.8}$ and $[\text{Cr-C}_4]\text{Cr}_3\text{C}_2=\text{Cr}_{40}\text{C}_{60}$ for Cr-DLC coatings with high corrosion resistance and electrical conductivity. Here, we introduce the percolation theory into the Cr-C system, to reveal the conduction mechanism of Cr-DLC coatings (the synergistic effect of sp^2 hybrid bonds and conductivity of Cr element itself).

There are three types of hybrid bonds in DLC coatings: sp , sp^2 and sp^3 ^[45]. Among them, the content of sp hybrid bonds is negligible. For the sp^3 hybrid bonds, all four valence electrons interact with electrons of the outer atoms to form strong σ bonds and a hybrid orbital with tetrahedral configuration. For the sp^2 hybrid bonds, only three valence electrons are paired with the electrons of the outer atoms to form strong σ bonds, forming a triangular hybrid orbit, while the fourth valence electron forms a weak π bond in the plane perpendicular to the hybrid orbit. The σ bonds in sp^2 and sp^3 configurations respectively forms the occupied σ state and unoccupied σ^* state in the valence band and conduction band, with a wide $\sigma-\sigma^*$ band gap between the two. However, the π bonds in sp^2 configurations form the occupied π state and unoccupied π^* state in the valence band and conduction band, respectively, with a narrower $\pi-\pi^*$ band gap between them. When the content of sp^2 hybrid bonds

increases, π states form tail states that link valence band and conduction band in the mobility gap, which leads to the π electron density delocalization and the electron conduction. Therefore, increasing the sp^2 hybrid bond content is an effective way to improve the electrical conductivity of Cr-DLC coatings. Additionally, Krauser *et al.*^[46] pointed out that, when the content of sp^2 hybrid bonds exceeds the bond percolation threshold of 0.388 for the three-dimensional diamond lattice configuration, a bond percolation conductive channel lapped by sp^2 hybrid bonds can be formed in the amorphous carbon network, which can significantly improve the conductivity of amorphous carbon coatings.

In Cr-DLC coatings, an appropriate amount of Cr catalyzes the formation of sp^2 hybrid bonds. As shown in Fig.6 (the data are from references^[3,47-49] and the present work), the sp^2 hybrid bond content in Cr-DLC coatings generally shows an increasing tendency as the Cr content increases, and after reaching maximum near the composition of the cluster formula $Cr_{22.2}C_{77.8}=[Cr-C_4]CrC_3$, the sp^2 hybrid bond content falls. It is then confirmed that the maximum sp^2 content is indeed reached near the proposed composition of $Cr_{22.2}C_{77.8}=[Cr-C_4]CrC_3$, as already mentioned in the discussion of Table 2. What is more important is that the sp^2 contents near this composition are all above the critical percolation threshold 0.388 of three-dimensional diamond lattice. Under this composition, a bond percolation conductive pathway is formed in the amorphous carbon network, which greatly enhances the electrical conductivity of Cr-DLC coatings. Experimentally, the electrical resistivity of the Cr-DLC coating near $Cr_{22.2}$ is in the order of $10^{-4} \Omega \cdot cm$ (see the solid line in Fig.1), far exceeding the year 2020 objective of the bipolar plates in proton exchange fuel cell set by US DOE^[40].

Further increasing the Cr doping content causes a

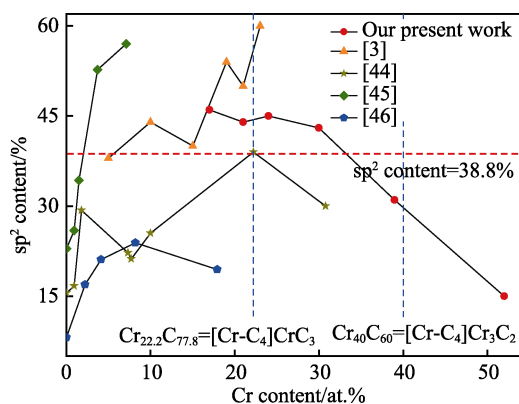


Fig.6 Relationship between Cr doping content and structure of Cr-DLC coatings (The data are taken from [3,47-49] and from the present work. The two dotted vertical lines point to the Cr doping contents of the cluster formulas $Cr_{22.2}C_{77.8}=[Cr-C_4]CrC_3$ and $Cr_{40}C_{60}=[Cr-C_4]Cr_3C_2$, and the dotted horizontal line marks the bond percolation threshold 0.388 of the three-dimensional diamond lattice.)

decrease in the sp^2 hybrid bonds, apparently by forming abundant Cr—C bonds. As can be noted from Fig.6, at 39at.%Cr(close to $Cr_{40}C_{60}=[Cr-C_4]Cr_3C_2$), the content of sp^2 hybrid bonds is 31.0%, below the percolation threshold 38.8. Nevertheless, this high Cr coating is still fairly conductive as can be seen in Figs.2 and 3. Such a contradiction can be addressed by the site percolation condition assured by the conductive Cr atoms in DLC.

The Cr element itself has excellent electrical conductivity, $1.29 \times 10^{-5} \Omega \cdot cm$ at room temperature. In Cr-DLC coatings, the doping of Cr element causes the Fermi level to migrate to the conduction band, and the valence electrons of the Cr element are delocalized and move along the sp^2 hybrid bond to form long-range electron transport channels, thus improving the conductivity of Cr-DLC coatings. S. Meskinis *et al.*^[11] pointed out that the conductivity of Cu-DLC coatings depends on their conductive volume fraction (Cu element volume fraction). When the volume fraction of Cu atoms exceeds the critical percolation volume, a percolation conductive pathway will be formed in the amorphous carbon network, and the percolation conductive pathway can be regarded as the main charge transfer mechanism in Cu-DLC coatings.

Following Monte Carlo simulations, the critical parameters for the formation of percolation pathways in three-dimensional lattice structures are obtained [43] and listed in Table 3. The parameters include p_c^{bond} and p_c^{site} , denoting respectively the percolation thresholds of bond percolation and site percolation. The percolation threshold value depends on the lattice configuration, which limits the application of the percolation theory in disordered systems and stochastic-geometry situations. In 1970, Scher and Zallen^[43] proposed the concept of critical volume fraction, $\phi_c = \nu p_c^{site}$, for the site percolation in stochastic geometric systems, which is numerically equivalent to the product of the percolation threshold and the packing factor of stochastic geometric structures. The concept of critical volume fraction makes the determination of long-range connectivity in the system no longer dependent on its lattice configuration, and the critical volume fraction of the three-dimensional system is a constant, 0.146^[44].

Here, we introduce the percolation theory into the investigation of the conductive mechanism of Cr-DLC coatings. As already mentioned, our disordered system has an average coordination number of 4 so that the diamond lattice parameters can be reasonably used in our case. By comparing the volume fraction of doped Cr elements in the Cr-DLC coating system with the critical volume fraction in the three-dimensional diamond system, we can determine whether the percolation conductive channels with long-range connectivity can be formed in the amorphous carbon network and reveal the conduction mechanism of Cr-DLC coatings.

Table 3 Coordination number N , packing factor ν , percolation threshold p_c^{bond} & p_c^{site} , critical bond number Np_c^{bond} (the critical value of the average number of connected bonds per site) and critical volume fraction of the three-dimensional lattice νp_c^{site} [43]

Structure	Coordination number (N)	Packing factor (ν)	p_c^{bond}	p_c^{site}	Np_c^{bond}	νp_c^{site}
FCC	12	0.7405	0.119	0.198	1.43	0.147
BCC	8	0.6802	0.179	0.245	1.43	0.167
SC	6	0.5236	0.247	0.311	1.48	0.163
Diamond	4	0.3401	0.388	0.428	1.55	0.146

We consider the atoms in Cr-DLC coatings as hard spheres, and the Cr and C atoms have a Goldschmidt radius R_{Cr} and R_{C} of 0.128 nm and 0.092 nm, respectively. These values have been confirmed by the measured bond lengths as already mentioned earlier in this paper. The atomic volumes are $V_{\text{Cr}} = 4\pi R_{\text{Cr}}^3/3 \approx 8.78 \times 10^{-3} \text{ nm}^3$ and $V_{\text{C}} = 4\pi R_{\text{C}}^3/3 \approx 3.26 \times 10^{-3} \text{ nm}^3$. Assuming that the atomic volume does not change in Cr-DLC, the average atomic volume V_a is calculated following $V_a = (f_{\text{Cr}}V_{\text{Cr}} + f_{\text{C}}V_{\text{C}})/\nu$, where f_{Cr} and f_{C} respectively represent the atomic percentages of Cr and C elements in Cr-DLC system, and ν represents the packing factor of the studied system ($\nu=0.3401$ in the diamond configuration). The average atomic volumes of the formulated structure units $[\text{Cr-C}_4]\text{CrC}_3$ and $[\text{Cr-C}_4]\text{Cr}_3\text{C}_2$ are respectively $V_a^{[\text{Cr-C}_4]\text{CrC}_3} = 1.312 \text{ nm}^3$ and $V_a^{[\text{Cr-C}_4]\text{Cr}_3\text{C}_2} = 1.609 \text{ nm}^3$. The volume fractions occupied by Cr atoms in the two structural units are respectively $\Phi_{\text{Cr}}^{[\text{Cr-C}_4]\text{CrC}_3} = f_{\text{Cr}}V_{\text{Cr}}/V_a^{[\text{Cr-C}_4]\text{CrC}_3} \approx 0.148$ and $\Phi_{\text{Cr}}^{[\text{Cr-C}_4]\text{Cr}_3\text{C}_2} \approx 0.218$, which are all larger than 0.146, the critical volume fraction of three-dimensional system. Therefore the percolation conductive channel can be formed in the amorphous carbon network, thereby enhancing the electrical conductivity of Cr-DLC coatings.

4 Conclusions

This paper presents a full coverage on both the modeling of Cr-doped DLC structures and on the interpretation of their electrical and corrosion behavior. The Cr-DLC amorphous structure is described, in terms of the cluster-plus-glue-atom model, as a local structural unit consisting of a nearest-neighbor cluster $[\text{Cr-Cr}_4]$ plus a few glue atoms to reach electron orbital saturation. Two cluster formulas $[\text{Cr-C}_4]\text{CrC}_3 = \text{Cr}_{22.2}\text{C}_{77.8}$ and $[\text{Cr-C}_4]\text{Cr}_3\text{C}_2 = \text{Cr}_{40}\text{C}_{60}$ are then proposed. An experimental verification is conducted. Thin films are prepared by arc deposition and are measured for Cr concentration, bond content, electrical resistance, and corrosion resistance. After a thorough analysis on the experimental data both from our own and from the literature, it is pointed out that the coatings of chemical compositions close to the proposed ones do show simultaneous low electrical resistivity

(down to $10^{-4} \Omega\cdot\text{cm}$) and superior corrosion resistance (corrosion potential above 0.4 V and corrosion current density $\sim 10^{-2} \mu\text{A}/\text{cm}^2$). The synergetic electrical and corrosion behavior is discussed within the framework of sp^2 bond content and of the percolation theory.

The present work not only validates the composition design method using the cluster-plus-glue-atom model, but also supports the use of the specified Cr-DLC coatings in dipolar plates in proton exchange membrane fuel cell.

References

- [1] LI X G, SABIR I. Review of bipolar plates in PEM fuel cells: Flow-field designs[J]. Int j hydrog energy, 2005, 30(4): 359-371.
- [2] MAKKUS R C, JANSSE A H N, DE BRUIJN F A, et al. Use of stainless steel for cost competitive bipolar plates in the SPFC[J]. J power sources, 2000, 86: 274-282.
- [3] WU B, LIN G, FU Y, et al. Chromium-containing carbon film on stainless steel as bipolar plates for proton exchange membrane fuel cells[J]. Int j hydrog energy, 2010, 35: 13255-13261.
- [4] WANG Z, FENG K, LI Z, et al. Self-passivating carbon film as bipolar plate protective coating in polymer electrolyte membrane fuel cell[J]. Int j hydrog energy, 2016, 41(13): 5783-5792.
- [5] LIU M, XU H F, FU J, et al. Conductive and corrosion behaviors of silver-doped carbon-coated stainless steel as PEMFC bipolar plates[J]. Int j miner metall mater, 2016, 23(7): 844-849.
- [6] GUDAITIS R, MEŠKINIS Š, ŠLAPIKAS K, et al. Piezoresistive and electrical properties of Cr containing diamond-like carbon films[J]. Surf coat technol, 2012, 211: 80-83.
- [7] CHANG Y Y, WANG D Y. Structural and electrical properties of Cr doped a-C:H films synthesized by a cathodic-arc activated deposition process[J]. Surf coat technol, 2006, 200(10): 3170-3174.
- [8] WONG H, FOONG Y M, CHUA D H C. Improving the conductivity of diamond-like carbon films with zinc doping and its material properties[J]. Appl surf sci, 2011, 257(22): 9111-9116.

- 9616-9620.
- [9] LIN Y H, LIN H D, LIU C K, et al. Structure and characterization of the multilayered Ti-DLC films by FCVA[J]. *Diam relat mat*, 2010, 19: 1034-1039.
- [10] LEE N R, JUN Y S, MOON K I, et al. Ti-doped hydrogenated diamond like carbon coating deposited by hybrid physical vapor deposition and plasma enhanced chemical vapor deposition[J]. *Jpn j appl phys*, 2017, 56: 035506.
- [11] MEŠKINIS Š, GUDAITIS R, VASILIAUSKAS A, et al. Piezoresistive properties of diamond like carbon films containing copper[J]. *Diam relat mat*, 2015, 60: 20-25.
- [12] ZENG L, HELGREN E, HELLMAN F, et al. Microstructure, magnetotransport, and magnetic properties of Gd-doped amorphous carbon[J]. *Phys rev B*, 2007, 75: 235450.
- [13] FERRARI A C, LIBASSI A, TANNER B K, et al. Density, sp^3 fraction, and cross-sectional structure of amorphous carbon films determined by X-ray reflectivity and electron energy-loss spectroscopy[J]. *Phys rev B*, 2000, 62(16): 11089.
- [14] DORFMAN B F. Critical parameters of percolation in metal-dielectric diamond-like composites of atomic scale[J]. *Thin solid films*, 1998, 330(2): 76-82.
- [15] ROBERTSON J, O'REILLY P. Electronic and atomic structure of amorphous carbon[J]. *Phys rev B*, 1987, 35(6): 2946.
- [16] ANGUS J C, JANSEN F. Dense "diamond like" hydrocarbons as random covalent networks[J]. *J vac sci technol A*, 1988, 6(3): 1778-1782.
- [17] LI X, ZHANG D, LEE K R, et al. Effect of metal doping on structural characteristics of amorphous carbon system: A first-principles study[J]. *Thin solid films*, 2016, 607: 67-72.
- [18] SINGH V, PALSHIN V, TITTSWORTH R C, et al. Local structure of composite Cr-containing diamond-like carbon thin films[J]. *Carbon*, 2006, 44(7): 1280-1286.
- [19] DONG C, WANG Q, QIANG J B, et al. From clusters to phase diagrams: Composition rules of quasicrystals and bulk metallic glasses[J]. *J phys D: Appl phys*, 2007, 40(15): R273.
- [20] WANG Z R, QIANG J B, WANG Y M, et al. Composition design procedures of Ti-based bulk metallic glasses using the cluster-plus-glue-atom model[J]. *Acta mater*, 2016, 111: 366-376.
- [21] ZACHARIASEN W H. The atomic arrangement in glass[J]. *Journal of the American Chemical Society*, 1932, 54(10): 3841-3851.
- [22] BERNAL J D. A geometrical approach to the structure of liquids[J]. *Nature*, 1959, 183(4655): 141.
- [23] GASKELL P H. A new structural model for transition metal-metalloid glasses[J]. *Nature*, 1978, 276(5687): 484.
- [24] MIRACLE D B, SANDERS W S, SENKOV O N. The influence of efficient atomic packing on the constitution of metallic glasses[J]. *Philos mag*, 2003, 83(20): 2409-2428.
- [25] SHENG H W, LUO W K, ALAMGIR F M, et al. Atomic packing and short-to-medium-range order in metallic glasses[J]. *Nature*, 2006, 439(7075): 419.
- [26] HAN G, QIANG J, LI F, et al. The e/a values of ideal metallic glasses in relation to cluster formulae[J]. *Acta mater*, 2011, 59(15): 5917-5923.
- [27] DONG D, DONG C. Composition interpretation procedures of bulk metallic glasses via example of $Cu_{64}Zr_{36}$ [J]. *J non-cryst solids*, 2017, 460: 125-129.
- [28] ANDERSSON M, HÖGSTRÖM J, URBONAITE S, et al. Deposition and characterization of magnetron sputtered amorphous Cr-C films[J]. *Vacuum*, 2012, 86(9): 1408-1416.
- [29] OLOVSSON W, ALLING B, MAGNUSON M. Structure and bonding in amorphous $Cr_{1-x}C_x$ nanocomposite thin films: X-ray absorption spectra and first-principles calculations[J]. *J phys chem C*, 2016, 120(23): 12890-12899.
- [30] FAN X, DICKEY E C, PENNYCOOK S J. Study of chromium-doped diamond-like carbon by z-contrast imaging and electron energy loss spectroscopy[J]. *MRS online proceedings library archive*, 1999, 45: 593.
- [31] SANTANA J A C, SINGH V, PALSHIN V, et al. Negative magnetoresistance in Cr-containing diamond-like carbon-based heterostructures[J]. *Appl phys A*, 2010, 98(4): 811-819.
- [32] WU Z, TIAN X, GUI G, et al. Microstructure and surface properties of chromium-doped diamond-like carbon thin films fabricated by high power pulsed magnetron sputtering[J]. *Appl surf sci*, 2013, 276: 31-36.
- [33] GAYATHRI S, KUMAR N, KRISHNAN R, et al. Influence of Cr content on the micro-structural and tribological properties of PLD grown nanocomposite DLC-Cr thin films[J]. *Mater chem phys*, 2015, 167: 194-200.
- [34] WANG Q, ZHOU F, DING X, et al. Structure and water-lubricated tribological properties of Cr/a-C coatings with different Cr contents[J]. *Tribol int*, 2013, 67: 104-115.
- [35] JELINEK M, ZEMEK J, VANDROVCOVÁ M, et al. Bonding and bio-properties of hybrid laser/magnetron Cr-enriched DLC layers[J]. *Mater sci eng C*, 2016, 58: 1217-1224.
- [36] ZOU C W, WANG H J, FENG L, et al. Effects of Cr concentrations on the microstructure, hardness, and temperature-dependent tribological properties of Cr-DLC coatings[J]. *Appl surf sci*, 2013, 286: 137-141.
- [37] GOU W, CHU X, LI G. Structure and properties of Cr-containing hydrogenated amorphous carbon films synthesized by filtered cathodic vacuum arc system[J]. *Plasma process polym*, 2007(s1): 207.
- [38] DAI W, WU G, WANG A. Preparation, characterization and properties of Cr-incorporated DLC films on magnesium alloy[J]. *Diam relat mat*, 2010, 19(10): 1307-1315.

- al. Instabilities in crystallization and magnetic behavior of Fe-Si-B amorphous alloys[J]. Materials research bulletin, 2004, 39(2): 231-236.
- [51] SU C, CHEN Y, YU P, et al. Linking the thermal characteristics and mechanical properties of Fe-based bulk metallic glasses[J]. Journal of alloys and compounds, 2016, 663: 867-871.
- [52] GUO W, CHOI P P, SEOL J B. Amorphous phase separation in an Fe-based bulk metallic glass[J]. Materials letters, 2017, 190: 161-164.
- [53] 李彦灼, 汪卫华. 无序材料中的待解之谜——金属玻璃研究进展[J]. 自然杂志, 2013, 35(3): 157-165.
LI Y Z, WANG W W. Puzzles awaiting solutions in amorphous materials: Progress of research on metallic glasses [J]. Chinese journal of nature, 2013, 35(3): 157-165.
- [54] THOMAS H, THOMAS S, RAMANUJAN R V, et al. Swift heavy ion induced surface and microstructural evolution in metallic glass thin films[J]. Nuclear instruments and methods in physics research section B: Beam interactions with materials and atoms, 2012, 287: 85-90.
- [55] THOMAS S, THOMAS H, AVASTHI D K, et al. Swift heavy ion induced surface modification for tailoring coercivity in Fe-Ni based amorphous thin films[J]. Journal of applied physics, 2009, 105(3): 033910.
- [56] PILARCZYK W. The effect of high energy concentration source irradiation on structure and properties of Fe-based bulk metallic glass[J]. Applied surface science, 2016, 374: 359-364.
- [57] GUPTA A, CHAUHAN R S, AGARWAL D C, et al. Smoothing, roughening and sputtering: The complex evolution of immiscible Fe/Bi bilayer system[J]. Journal of physics D: Applied physics, 2008, 41(21): 579.
- [58] SUN J R, WANG Z G, WANG Y Y, et al. Study of local crystallization induced in FeSiNbZrB amorphous alloy by swift heavy ion (SHI) irradiation at room temperature[J]. Nuclear instruments and methods in physics research section B: Beam interactions with materials and atoms, 2013, 307: 486-490.
- [59] KANE S N, SATALKAR M, GHOSH A, et al. Electron-irradiation induced changes in structural and magnetic properties of Fe and Co based metallic glasses[J]. Journal of alloys and compounds, 2014, 615: s324-s327.
- [60] PAVLOVIČ M, MIGLIERINI M, MUSTAFIN E, et al. Radiation damage studies of soft magnetic metallic glasses irradiated with high-energy heavy ions[J]. Radiation effects and defects in solids, 2015, 170(1): 1-6.
- [61] KOTAGIRI G, MARKANDEYULU G, THULASIRAM K V, et al. Magnetoimpedance studies on ion irradiated $\text{Co}_{33}\text{Fe}_{33}\text{Ni}_7\text{Si}_7\text{B}_{20}$ ribbons[J]. Journal of magnetism and magnetic materials, 2016, 404: 79-82.

(上接第 10 页)

- [39] MA Y, DONG D, WU A, et al. Composition formulas of inorganic compounds in terms of cluster plus glue atom model[J]. Inorg chem, 2017, 218: 185.
- [40] DRIVE U S. Fuel cell technical team roadmap[M]. New York: US Drive Partnership, 2013: 1-26.
- [41] VISWANATHAN S, MOHAN L, BERA P, et al. Corrosion and wear behaviors of Cr-doped diamond-like carbon coatings[J]. J mater eng perform, 2017, 26(8): 3633-3647.
- [42] WANG Q, ZHOU F, ZHOU Z, et al. Effect of titanium or chromium content on the electrochemical properties of amorphous carbon coatings in simulated body fluid[J]. Electrochim acta, 2013, 112: 603-611.
- [43] ZALLEN R. The physics of amorphous solids[M]. London: John Wiley & Sons, 2008.
- [44] FITZPATRICK J P, MALT R B, SPAEPEN F. Percolation theory and the conductivity of random close packed mixtures of hard spheres[J]. Phys lett A, 1974, 47(3): 207-208.
- [45] ROBERTSON J. Diamond-like amorphous carbon[J]. Mater sci eng R: Rep, 2002, 37(4-6): 129-281.
- [46] KRAUSER J, NIX A K, GEHRKE H G, et al. Highly conductive ion tracks in tetrahedral amorphous carbon by irradiation with 30 MeV C60 projectiles[J]. New j phys, 2011, 13(8): 083023.
- [47] JELINEK M, ZEMEK J, VANDROVCOVÁM, et al. Bonding and bio-properties of hybrid laser/magnetron Cr-enriched DLC layers[J]. Mater sci eng C, 2016, 58: 1217-1224.
- [48] JELINEK M, KOCOUREK T, ZEMEK J, et al. Chromium-doped DLC for implants prepared by laser-magnetron deposition[J]. Mater sci eng C, 2015, 46: 381-386.
- [49] JELINEK M, PISARIK P, KOCOUREK T, et al. Preliminary comparative study of laser-prepared DLC and Cr-doped DLC for bacteria adhesion[J]. Appl phys A, 2014, 116(3): 1437-1443.